INSOLATION EFFECTS ON THE MOON: HIGH TOPOGRAPHIC SLOPE OBSERVATIONS FROM THE LRO LEND AND LOLA INSTRUMENTS. T.P. McClanahan[1], I.G. Mitrofanov[2], W.V Boynton[3], G. Chin[1], R.D. Starr[4], L.G. Evans[5], G. Droege[3], A. Sanin[2], J. Garvin[1], J. Trombka[1], Astrochemistry Laboratory, NASA Goddard Space Flight Center, Greenbelt, MD 20771, (timothy.p.mcclanahan@nasa.gov), [2]Institute for Space Research, RAS, Moscow 117997, Russia, [3]Lunar and Planetary Laboratory, Univ. of Arizona, Tucson AZ, [4]Catholic Univ. of America, Washington DC, [5]Computer Sciences Corporation, Lanham MD 20706.

Introduction: The extremely low temperatures in the Moon's polar permanent shadow regions (PSR) has long been considered a unique factor necessary for entrapping volatile Hydrogen (H) [1,2]. However, recent discoveries indicate some H concentrations lie outside PSR, suggesting other geophysical factors may also influence H distributions [3-5]. In this study we consider insolation and its resulting thermal effects as a loss / redistribution process influencing the Moon's near-surface < 1m volatile H budget.

To isolate regional (5° latitude band) insolation effects we correlate two data sets collected from the ongoing, 1.5 year long mapping mission of the Lunar Reconnaissance Orbiter (LRO) [6]. Epithermal neutron mapping data from the Lunar Exploration Neutron Detector (LEND) is registered and analyzed in the context of slope derivations from Lunar topography maps produced by the Lunar Observing Laser Altimeter (LOLA) [7][8]. Lunar epithermal neutrons are inferred to be direct geochemical evidence for near-surface H due to the correlated suppression of surface leakage fluxes of epithermal neutrons with increased H concentration. Regional suppressions of neutrons seen in LEND maps are considered localized evidence of H concentration increase in the upper 1m of the Lunar surface. To quantify spatially localized insolation effects, LEND data are averaged from sparsely distributed pixels, classed as a function of the LOLA slope derivations described below.

Background: Thermal effects of insolation are primarily a function of a cosine process $a = i \cos \Theta$, which predicts the effective solar irradiation a, incident to a given surface as a function of its angular orientation Θ, to the source solar irradiation, i. Θ is locally a function of several variables including combined: seasonal, diurnal, topographic, latitude and regolith compositional effects which induces locally dependent and time variable thermal conditions. Given the Moons low obliquity, increased latitude predictably attenuates a, and is correlated with decreased near-surface temperatures towards the poles [5]. Topographic variance influences a slopes relative orientation to incident solar irradiation thus inducing local thermal conditions. Regolith compositional effects e.g, granularity and composition influence the thermal conductivity of the regolith near surface thus influencing the thermal gradient.

In terrestrial polar regimes insolation effects on near surface distributions of water are readily contrasted in pole facing (PF) vs. equator facing (EF) slopes. EF slopes overall receive greater expected a, due to their generally higher solar incident elevation angles vs. PF slopes. The contrasting a, thermal effects, induce greater dessication rates in near-surface EF slopes vs. equivalent PF slopes. Local PF vs. EF differences in a, are also maximized with increased slope. In this experiment we postulate similar Lunar effects and implement these conditions using LOLA to identify pixels that locally maximize a contrast and evaluate epithermals neutrons from LEND maps.

Methods: LEND maps were prepared using primary mapping mission derived LEND data (DLD) Sept 15, 2009 to July 25, 2010. North and South polar maps +/-45° to poles are produced using a 7200x7200 pixel, 0.4 km resolution map. The mapping kernel is a 2-D, 20km diameter uniform area mapping disk which maps each sample by scaling the kernel with the integral of LEND's ~four, 1 Hz rate, collimated sensors.

Two polar (n,s) LOLA, 0.4 km resolution digital elevation models (DEM) were selected from the LOLA Planetary Data System (PDS release, Dec 15, 2010) files: ldem_45(s,n)_400m.img, $\mathbf{m}$. Image directional topographic gradients are derived, $\mathbf{g_{x,y}} = \mathbf{N}(0,0.83)'_{x,y} * \mathbf{m}$, where $\mathbf{N'}$ is two convolution kernels containing the (x,y) image coordinate directional 1st derivatives of a 2x2 km (5x5) pixel, 0. centered Gaussian, σ=0.83km. Topographic slope $\mathbf{s} = \tan^{-1}(|\mathbf{g}|)$.

Slope orientation map, $\mathbf{\Phi} = \cos^{-1}(\mathbf{uv}/|\mathbf{u}||\mathbf{v}|)$, defines a given $\mathbf{s}$ pixel's angular orientation with respect to the pole facing direction. For each map pixel i, $\mathbf{u_i}$ = directional vector to the pole pixel in image space (x,y). $\mathbf{v_i}$ = slope directional vector $[\mathbf{g}_{x,i}, \mathbf{g}_{y,i}]$. The transformation yields a linearized continuous map, range [0° to 180°] of slope orientation, Φ. Φ = 0° = pole facing $\Rightarrow$ 90°=(east, west) facing $\Rightarrow$ 180° = equator facing. Importantly, this is a scale invariant transformation mapping all crater slopes to a common scale. These transforms facilitate geomorpholgically based, selection and sparse averaging of LEND pixels, Figure 1. Due to polar trajectories, LEND map uncertainties also increase towards the equator, however higher low lati-

tude uncertainties are generally offset by higher PF, EF averaging areas / 5° latitude bin.

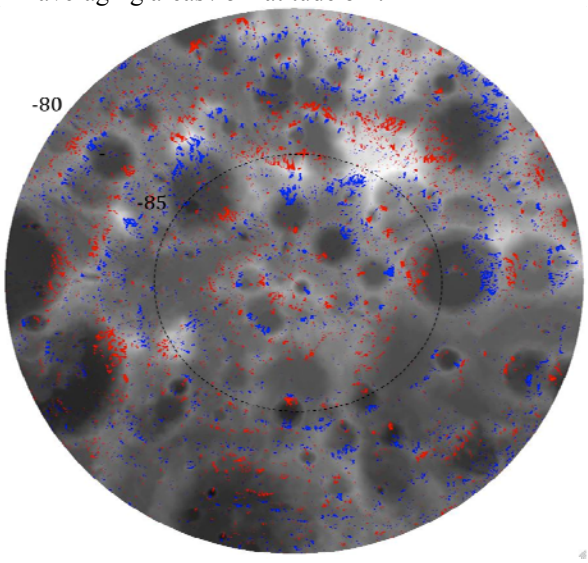

Figure 1: LOLA south pole centered DEM [8], (-80:-90). Elevation (*greyscale*). High slopes > 15°(*color*). Pole facing (Φ:0-10) (*blue*), Equator facing (Φ:170-180) (*red*). Pixels for LEND *f*(PF, EF) >= 15° slopes.

Results: Figures 2, 3 illustrate the north, south +/- 45° to pole comparisons of LEND pixels sparsely averaged from each 5° latitude bin. High slopes >= 15° are analyzed to maximize expected PF (*blue*) vs EF (*red*) differences in *a*. 15° is the upper slope threshold determined via pilot study for assuring each data class is aerially sufficiently populated. Within each latitude bin, LEND epithermal averages are determined as LOLA, *f*(PF = (Φ <= 10), EF = (Φ >= 170), **s** >= 15°).

North results indicate epithermal neutron rate averages collected over high EF slopes are consistently 0.01 to 0.02 cps higher than averages collected over PF slopes from 50° latitude to NP. South pole results quantify similar EF vs. PF differences 0.01 to 0.02 cps for results -55° to SP. Statistical t-tests of the high latitude PF < EF epithermal avg. rate means indicate significant differences, μ_{PF} vs μ_{EF}, α=0.05.

Conclusion: The consistent epithermal rate (PF vs. EF) differences for both high latitude results +/- > 55° latitude suggest support for insolation effects as an important factor influencing dependent H loss processes for lunar near-surfaces < 1m in high slopes.

We assume high slope slip faces tend to be comparatively, younger and rougher with thinner regolith deposits than low slope surfaces and consider the following two postulates. 1) There exists a continuum of solar incidence angles between similar high PF vs. EF slopes. For fixed slope and roughness conditions this induces greater frequency and areal shadowing of small pockets and subsequent thermal H entrapment effects in PF slopes vs EF. 2) If high slope regolith is sufficiently thick, active zones similar to terrestrial permafrost regimes may be produced in which volatile H mobility and depletion is a function of the local diffusive pentetration of heat into regolith via local *a*. Local *a*, heat penetration would be conditionally maximized in high solar elevations near summer solstice.

However, these are macro scale results (5° lat bins) and there are likely other important combinations of geophysical factors influencing H budgets at smaller scales, lower latitudes and polar contexts to consider.

Lastly, we thank the LEND, LOLA and LRO teams for their instrument and spacecraft contributions to this and other ongoing Lunar research.

References: [1] Arnold (1979) *JGR*, #84, 5659-5668 [2] Feldman et al.,(2001) *JGR*, 106-E10, 23231-23251 [3] Mitrofanov et al.(2010) *Science*, 330-6003, 483-486 [4] Pieters et al.(2009) *Science*, 326(5952), 568-572 [5] Paige et al. (2010) *Science*, 330-6003, 479-482 [6] Chin et al. (2007) *Sp. Sci. Rev.*, 150(1-4), 125-160 [7] Mitrofanov et al.(2010) *Sp. Sci. Rev., 150(1-4),* 183-207. [8] Smith et al.(2010) *Sp. Sci. Rev., 150(1-4)*.

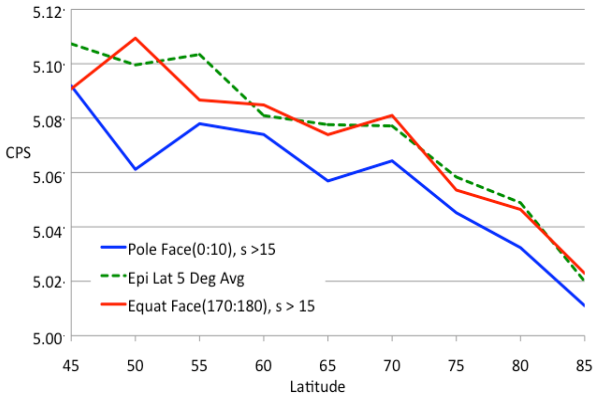

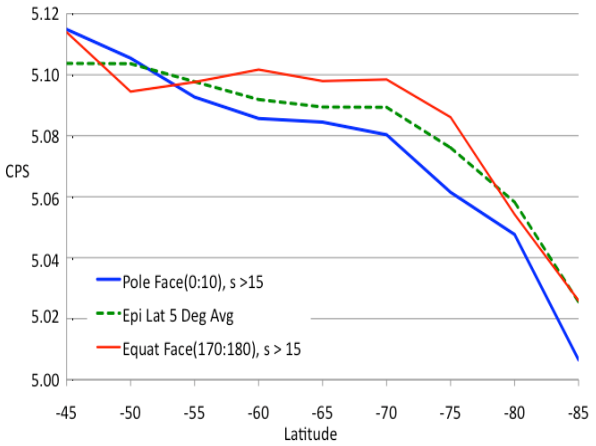

Figure 2(top): North Pole facing (*blue*: 0-10) vs. Equator facing slopes (*red*: 170-180), Latitude band average (*green*) **Figure 3(bottom)**: South Pole facing vs. Equator Facing slopes (as described in Fig 2)